

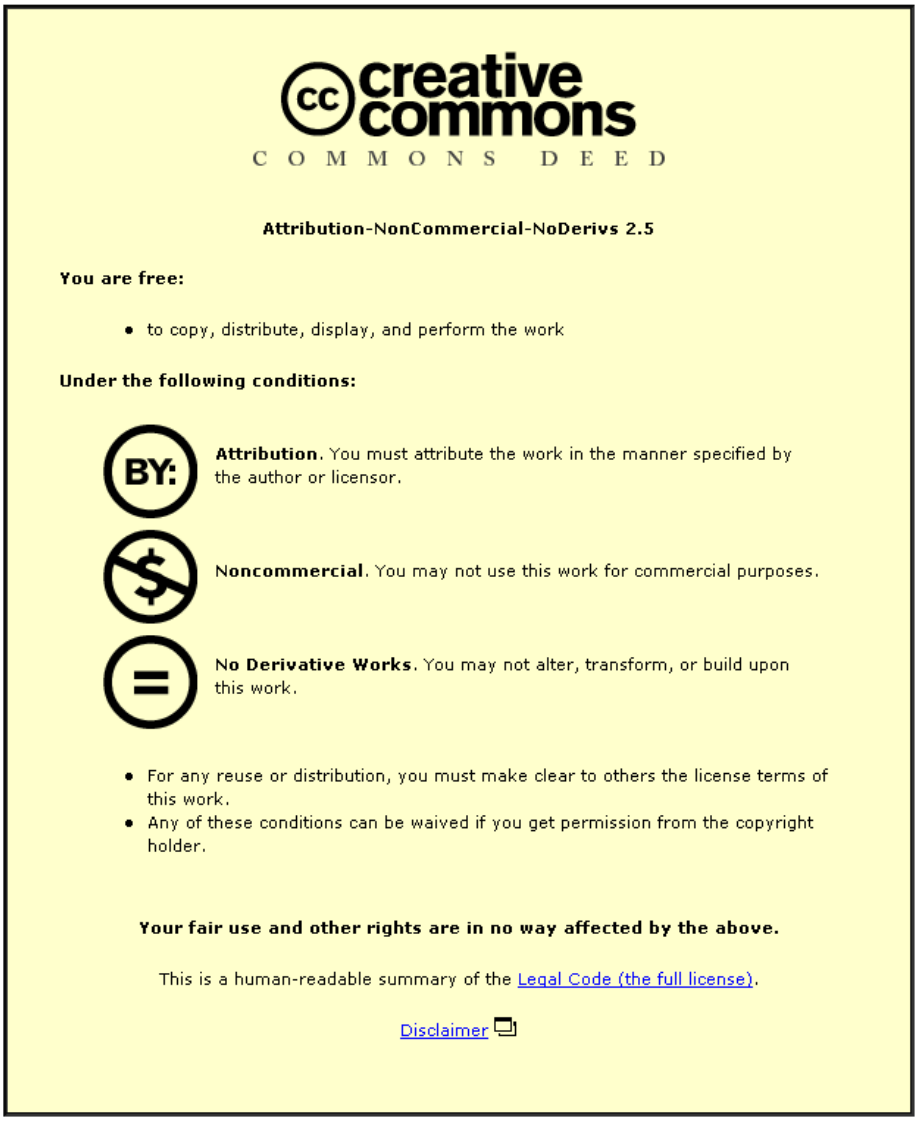

creative commons

COMMONS DEED

**Attribution-NonCommercial-NoDerivs 2.5**

**You are free:**

- to copy, distribute, display, and perform the work

**Under the following conditions:**

**Attribution**. You must attribute the work in the manner specified by the author or licensor.

**Noncommercial**. You may not use this work for commercial purposes.

**No Derivative Works**. You may not alter, transform, or build upon this work.

- For any reuse or distribution, you must make clear to others the license terms of this work.
- Any of these conditions can be waived if you get permission from the copyright holder.

**Your fair use and other rights are in no way affected by the above.**

This is a human-readable summary of the Legal Code (the full license).

Disclaimer

# Influence of diurnal and seasonal temperature variations on the detection of corrosion in reinforced concrete by Acoustic Emission.

*Richard Lyons*[*]*, Matthew Ing, Simon Austin*

*Centre for Innovative Construction Engineering,*
*Loughborough University, Leicestershire, LE11 3TU*

**Abstract**

Chloride rich reinforced concrete prisms were coupled to chloride free prisms and exposed to diurnal and seasonal temperature cycles typical of those found in the UK. Acoustic Emissions (AE) and galvanic currents were continuously monitored and correlated with ambient temperature. AE and galvanic currents were found to emulate the evolution of temperature in the diurnal cycles, although no specific relationship between AE and galvanic current could be obtained. The influence of seasonal variations in galvanic current had no obvious influence on AE Energy per second over the range of corrosion rates studied. The findings suggest that AE is more sensitive to short term (diurnal) changes in corrosion rates than the longer (seasonal) effects. It was hypothesised that this is due to transitory changes in the internal microclimate of the concrete.

*Keywords:* Steel reinforced concrete, thermal cycling, acoustic emission

## 1. Introduction

In most instances reinforcing steel remains in a passive state for the duration of the structure's life, attributable to the high alkalinity of the soluble constituents in the concrete pore water and the physical barrier against aggressive species, provided by the cover. However, penetration of chlorides through the cover and or neutralisation of the pore water due to carbonation are the two primary factors that can instigate rebar corrosion, leading to a loss of steel section and or loss of bond.

The rate at which the subsequent corrosion reaction will proceed depends primarily upon the ambient temperature, as expressed by the Arrhenuis equation [1], internal relative humidity (RH) and oxygen content [2-4]. In real concrete structures, the internal RH and temperature are continuously changing within the concrete [3,5], evolving with the seasonal and diurnal cycles of the environment and in the case of exposed concrete, the internal RH is influenced by wetting and drying [6,7]. Thus the rate of corrosion is also a non-stationary phenomenon, in continual non-equilibrium with the environmental dynamic processes.

Overall, the effect of temperature on corrosion rates is a complex one but generally corrosion rates increase with increasing temperature. As a rule of thumb, a $10^{o}$C increase in temperature can double the corrosion rate [8] although the actual relationship will depend upon the interactions of the other related parameters, also influenced by temperature, such as internal resistance, oxygen diffusion, oxygen

content in the pores, changes in the free chloride content and alkalinity of the pore solution [3].

### *1.1 Scope of study*

Detection of rebar corrosion in concrete before external visual signs become apparent may provide a critical advantage for any corrosion detection method. Such early warnings might enable an effective and efficient management of the concrete degradation, avoiding sudden costs and closures. Acoustic emission (AE) is a promising non-destructive test technique, which has the potential for detecting the very early stages of corrosion, before external visual damage occurs [9,10] and is based on detection of the rapid release of energy within a material undergoing stress deformations. However, the link between AE measurement and active corrosion is not yet fully understood, certainly not enough to apply this technique successfully to detect reinforcement corrosion on site. Consequently, the focus of this work is to determine how variations in corrosion rate, induced by diurnal and seasonal temperatures, influence the ability of AE to detect low levels of corrosion in reinforced concrete.

### *1.2 Principles of AE*

Acoustic emissions are transient elastic stress waves resulting from a sudden release of elastic energy, caused by mechanical deformations, initiation, and propagation of microcracks, dislocation movement, phase transformations and other irreversible changes in a material [11]. The AE technique is widely used as a non-destructive

evaluation method for testing metallic or reinforced plastic vessels on-site [12] and more recently, has been applied to deteriorated concrete structures [13-14].

Over the past three decades, AE has been applied to monitor the initiation and propagation of aqueous corrosion. Research by Rettig and Felsen [15] reported a good correlation between AE counts and the corrosion of Fe and Al wire in hydrochloric acid, measured by the volume of hydrogen evolved. Furthermore, when Al was galvanically coupled to Fe, they reported that the increase in AE counts corresponded well to the increase in corrosion activity. Similar results were observed by Mansfeld and Stocker [16] who immersed aluminium alloys into a 3.5 % NaCl solution coupled to either Cu, Steel, Cd or Zn and were able to quantitatively relate the corrosion rate with AE emission. They reported that "AE activity is closely related to the current density and therefore pitting rate". More recently, Fregonese *et al* [17] studied the response of AE to the development of pitting corrosion on AISI 316L austentic stainless steel in a 3% NaCl solution. They demonstrated that AE was able to differentiate between the initiation and the propagation stage, where in the latter case the evolution of hydrogen bubbles were the reported cause of emission.

Research in AE techniques has also been extensively applied to concrete as a method of non-destructive testing [18-20]. Wu *et al* [21] reported AE to be "an effective method for studying the failure mechanism of concrete", supporting Hearn and Shield [22] who found AE to be a viable method of determining active crack growth in reinforced concrete structures. Furthermore, using source location, the cracks were located to within several centimetres with just two AE transducers. Li and Shah [23] successfully used AE on concrete under going uniaxial tensile tests, where the cause

of emission was the nucleation of microcracks. Whilst AE has been used as a method to monitor the structural integrity of beams placed under increasing loads with various levels of corrosion induced damage [24,25], AE has also been applied to the detection of steel reinforcement corrosion [26-29].

Corrosion-induced concrete damage has been detected by AE in laboratory specimens that are freely corroding and subjected to accelerated corrosion [10,29]. However, whilst it has been possible to correlate AE with the rate of aqueous corrosion [30], little work has been found that correlates AE to variations in the corrosion rate of steel reinforcement in concrete. Whilst limited work has investigated the environmental dynamics on corrosion rate in weathered concrete [3,5], there is no published evidence of the response of AE to these environmentally induced changes in corrosion rate, thus it is the aim of this work to investigate how AE responds to short term variations (diurnal cycles) and longer term changes (seasonal cycles) as part of the development of AE towards being a practical site technique.

## 2. Experimental Procedure

### *2.1 Overview of study*

The experimental procedure was divided into two elements: (i) Diurnal temperature testing of specimens exposed to a sheltered, outdoor climate in Loughborough, UK with continuous AE monitoring and, (ii) Physical modelling of a range of temperatures that may be encountered seasonally in the UK climate with continuous

AE monitoring of corroding specimens. The AE monitoring procedure was common for both experiments and is described in Section 2.7.

*2.2 Specimens for the Diurnal Temperature Testing*

For these experiments five prisms of dimensions 96 *x* 96 *x* 232 mm were cast out of a concrete containing 383 kg/m$^3$ of type 1 Portland cement, 670 kg/m$^3$ of fine aggregate and 1142 kg/m$^3$ of course aggregate with a water / cement ratio of 0.47. Each prism contained a 16 mm diameter deformed rebar (Grade 460) centrally placed with a cover of 40 mm. The rebar conformed to BS 4449:1997 with a carbon content of 0.25%. A further three specimens of identical dimensions and mix proportions were cast with the addition of 3% NaCl by weight of cement to promote corrosion. The final 30 mm of each rebar was wrapped in electrical insulation tape to prevent edge effects. Approximately 10 mm of the rebar protruded at both ends of the prisms to enable electrical connections to be made. The eight beams were water cured for 28 days and then left in an external sheltered environment for an arbitrary eight month period.

Prior to testing, a 10 mm slice of concrete was removed from the cast face of each prism using a diamond studded saw. The cut face of a prism containing NaCl (anode) was cemented to the cut face of a chloride-free prism (cathode) to produce the test beam. Three such beams were produced (Beams 1-3), together with a control (Beam 4), constructed from two chloride-free prisms. This produced a total of four beams of dimensions 172 *x* 96 *x* 232 mm as shown in Figure 1. The cementing was achieved by applying a thin layer of fresh cement slurry of water content 0.5 to both freshly cut surfaces and carefully sliding together in a sawing motion to prevent entrapment of

air. After 24 hours the samples were partially submerged in a water tank for seven days, with the chloride free prisms being partially exposed to the atmosphere. The water aided curing of the cement layer, but by only partially submerging the cathode it was intended that a differential aeration cell between the anode and cathode would be created, thus increasing the corrosion rate.

Upon removal from the water tank, a 100 Ω shunt resistor was connected between the ends of the two exposed rebars to create a galvanic couple between the two beams. Two coats of bitumen paint were applied to all four vertical faces of each beam to minimise water loss. Waterproof tape was attached to the exposed (top) face of the anode to ensure that evaporation and oxygen diffusion could only occur through the exposed cathode face. This allowed for the tape to be easily removed to undertake half-cell measurements. Sealing the beams in this manner was found to eliminate acoustic emissions generated by thermal cycling and significantly reduce water loss, thereby helping to maintain a galvanic current over a number of days. The physical dimensions of the Beams are greater than those used in the seasonal study in an attempt to maintain a sufficient water content at bar depth, without the need to immerse the specimens in water.

*2.3 Diurnal Test Procedure*

Beams 1-4 were each placed on two strips of wood, thus allowing airflow under the specimens and left exposed to an external environment sheltered from the wind and rain for a number of consecutive days.

*2.4 Specimens for Seasonal Temperature Testing*

For these experiments five prisms of dimensions 48 *x* 75 *x* 232 mm were cast using the same mix design and preparation procedure as described for Beams 1-4. Each prism contained a 16 mm deformed rebar with a 16 mm cover to the top, bottom and one side. Three further beams of identical dimensions were cast in a separate batch containing 316 kg/m$^3$ type 1 Portland cement, 652 kg/m$^3$ fine aggregate and 1212 kg/m$^3$ of course aggregate with a water / cement ratio of 0.57 and contained 3% NaCl by weight of cement to provoke corrosion of the reinforcement. The lower strength concrete mix was used to promote active corrosion of the rebar. The low cover and differential strengths were deliberately designed to maximise the galvanic flow.

*2.5 Seasonal Test Procedure*

A prism containing chloride was coupled to a chloride free prism to create a corrosion cell as shown in Figure 2. The coupled prisms will from hereon in be referred to as Cells to distinguish them from the Beams used in the diurnal study. Three such Cells were constructed (Cells 1 - 3) together with a control (Cell 4), consisting of two chloride free prisms. To minimise any effects of resistance control and to ensure a steady galvanic current, distilled water was continuously provided via wet wicks to the bottom of the anode and to the interface between the anode and cathode. The top wick provided a continuous ionic path between the anode and cathode and combined with the low cover thickness (16 mm), created a low resistance path for ionic transfer. Additionally the wet wicks served to increase the internal water content of the anode, thereby creating a differential aeration mechanism between the anode and cathode, thus increasing the potential difference, in addition to any effect the lower strength concrete may impart.

Cells 1-4 were placed in a custom-built climatic room set at 25, 15 and 5$^{o}$C (±1.5$^{o}$C) for 96 hours at each temperature (Test 1) and 5, 10 and 25$^{o}$C for 96 hours at each temperature (Test 2). The actual room temperature was recorded hourly using a data logger and any variations averaged over the day. The first test was run consecutively starting at 25$^{o}$C whereas the second test was started at 5$^{o}$C and increased in temperature. The refrigeration apparatus control limited the selection of set temperatures; hence the temperatures selected do not represent a specific time of year, but cover a broad range of the temperatures likely to be encountered annually in the UK. The cells were monitored continuously for acoustic emissions.

*2.6 Corrosion Rate Measurement*

Calculation of the galvanic current ($I_g$) from Beams 1-3 and Cells 1-3 (excluding the controls) was undertaken by logging the macro cell voltage across the 100 Ω shunt resistor once every second and then converted into current using Ohms Law. The polarity was arranged so that a positive $I_g$ corresponded to anodic corrosion, assuming that $I_g$ was restricted to the anode. Half-cell potentials were also recorded at the end of each temperature cycle using a copper / copper sulphate electrode (CSE). Half-cell potentials are commonly recorded in the field to assess the probability of corrosion activity. It is generally accepted that half-cell potential values more negative than –350 mV (CSE) indicate a 95% probability of corrosion occurring. Thus it was the intent in this work to record the half-cell potentials to provide a comparison between the AE and the accepted field method of assessing corrosion.

*2.7 Acoustic Emission Monitoring*

An AE 4-channel DiSP acquisition board, supplied and calibrated for this purpose by Physical Acoustics Ltd was used with piezoelectric transducers connected in series to an external buffer amplifier. Both hit and time driven data were recorded for post processing. PVC tape secured the transducers to each prism and the sensor / concrete interface was lubricated with grease to improve the coupling. PVC tape was used as it does not emit AE when stressed. The control beams were monitored to ensure that emission occurred as a result of corrosion and not from background sources in the testing environment. Emissions are recorded as *hits*, which are the transient waveforms of an AE signal that exceed a pre-set threshold. The hit will have specific parameters, for example the magnitude of the peak amplitude ($dB_{AE}$), duration (sec) of the signal and energy contained in the signal, calculated from the Modified Area Rectified Signal Envelope (MARSE) [8], a dimensionless quantity, relative to the energy gain set in the software. The number of hits is often used as a measure of the damage occurring to a material. However, the cumulative number of hits does not differentiate between high or low amplitude events, which can indicate the severity of the damage. Using the cumulative energy value the severity or activity of the source is more apparent as higher amplitude hits generally contain more energy.

## 3. Results

*3.1 Diurnal Temperature Effects*

*3.1.1 Galvanic Current*

The response of $I_g$ to the diurnal temperature variations is illustrated in Figure 3 for Beams 1-3 exposed to five consecutive diurnal cycles. The evolution of $I_g$ is shown to

resemble the changing ambient temperature with time, indicating a dependence of $I_g$ on temperature. However, a small time lag is evident between the maximum temperature and maximum $I_g$ probably due to thermal inertia effects.

Plotting hourly $I_g$ values against hourly ambient temperature (Figure 4) reveals a positive, linear relationship for all three beams indicating that an increase in temperature results in an increase in $I_g$. However, a degree of scatter exists, and an Arrhenuis relationship was not found indicating that the change in $I_g$ is not entirely attributable to a change in temperature and that a specific relationship between $I_g$ and temperature may not exist.

$I_g$ is also a function of the internal RH ($RH_{int}$) of the concrete, which in sheltered, exposed concrete, is largely influenced by temperature [31]. Whilst $RH_{int}$ was not measured, the masses of each specimen were recorded at the start and end of the five-day cycle and are presented in Table 1 together with the half-cell results taken at the same time. The results reveal that all four beams exhibited a decrease in mass, most probably due to evaporation of pore water. This loss of water may have affected $I_g$ by increasing the internal resistance, thus influencing any direct relationship with temperature. The evaporation of water was not responsible for any acoustic emission during the test, demonstrated by the control in Figures 5 & 6.

It is also evident from Figure 4 that the galvanic currents recorded from Beams 1-3 are very low. If it is assumed that the entire surface area of the rebar was corroding (100cm$^2$ nominal surface area), $I_g$ for Beam 1 equates to approximately 0.02µA/cm$^2$, suggesting that it is within the passive range (~0.1µA/cm$^2$). The AE results presented

in Figures 5 and 6 clearly suggest that this is not the case, however it is emphasised that very low rates of corrosion are being detected.

In Figure 4, it is apparent that differences in $I_g$ exist between the physically identical prisms. Whilst all three rebars are embedded in a chloride rich environment random geometrical heterogeneities, such as crevices, exist at the steel / concrete interface which act as a catalyst to corrosion initiation [32]. Once corrosion has initiated, González *et al* [32] suggest that the kinetics of the subsequent reaction will depend on the impact these geometrical heterogeneities and depassivation factors (such as the chloride ion or carbonation) have in addition to primary factors, such as oxygen concentration and the water content. Thus it is probable that the differences in the corrosion rates observed can be attributed to differences in geometrical heterogeneities and differing oxygen and water contents between the prisms.

*3.1.2 Acoustic Emission*

The response of AE to the diurnal temperature cycle is illustrated in Figure 5 showing AE hits per hour against ambient temperature. AE hits per hour have been plotted as a running average over a five-hour period to smooth out fluctuations in the data. It is clear that the AE activity emulates the temperature cycle, showing an increase and decrease in AE activity with temperature. Moreover, the control emitted virtually zero emissions over the entire test duration (~120 hours) strongly suggesting that the emissions from Beams 1-3 are as a result of corrosion as opposed to other mechanisms such as thermally induced AE or water loss. The clear distinction between the corroding beams and the control supports Dunn *et al* [26] who found that AE could distinguish between noble and active specimens.

However, whilst Figure 5 can be useful to identify AE activity and so corrosion, recording the energy contained in the AE hits may be used to provide a quantitative indication of damage occurring within the concrete as it considers both the amplitude and duration of a signal. The energy per hour for each of the four beams is shown in Figure 6, also presented as a running five hour average. The energy per hour for Beam 3 is clearly at a maximum during the warmer periods of the day, with Beams 1 and 3 exhibiting a greater degree of similarity. Comparing Figures 5 and 6, it is apparent that most of the energy from Beam 3 must be contained in a few of the hits as there is a large difference between the number of hits per hour relative to energy per hour. Such high-energy hits are typically of greater amplitude resulting in a few hits contributing to the majority of the energy in a hour period. Higher amplitude AE may be indicative of larger micro fracture.

Whilst the rate and energy of emissions generally increases with temperature, the magnitude of these emissions does not appear to be related to a specific $I_g$ (Figure 7) or maximum temperature, probably as the energy of the AE is not directly attributable to $I_g$ but a function of the material properties of the concrete [9], the co-efficient of expansion of the oxide, the frequency response of the transducer, the distance from the source of the emission (attenuation) and the number of simultaneous fractures occurring. Thus, the total AE energy recorded over a finite period does not relate to a specific $I_g$ or temperature but as shown in Figures 5 & 6, can only indicate the periods at which the corrosion activity is increased.

AE obtained during the coolest part of the diurnal cycles is shown in Figure 6 to be dramatically lower than at the warmer periods, but in nearly all cases remains greater than the control. Moreover, from the data presented, there is no minimum temperature below which AE is undetected and while the minimum temperature in each cycle is different, the minimum AE values remained fairly constant or at least above a minimum level.

From this work it is evident that corrosion is more easily detectable using AE during the warmer periods of the day, coinciding with the maximum temperature, although providing the monitoring period is of sufficient duration, corrosion of reinforcing steel in concrete is detectable at all times throughout the 24-hour cycle.

Independent of the time of day of testing, care should be taken in interpreting data due to the natural variations that occur in the magnitude of energy expelled during micro fracture. Such random occurrences are accentuated by the low corrosion rate where the data rate is inherently low, requiring only a few high-energy emissions to dominate the results as illustrated by Beam 3.

*3.1.3 Half-cell potentials*

The half-cell results, presented in Table 1 indicate that over the course of the five-day period, the electrochemical potential of the rebars became less negative and in the case of Beam 1, increased to a value suggesting that the rebar was approaching nobility (-353 mV), where the transition between active and noble steel is defined as –350 mV CSE. Clearly comparing the AE data to the control, it is evident that

corrosion was occurring, independently verified by a positive $I_g$. The reduction in potential may be attributable to the reduction in water content.

*3.2 Seasonal Temperature Effects*

It has been shown from the diurnal results that $I_g$ varies in response to diurnal temperature fluctuations; hence each prism will have a minimum and maximum $I_g$ influenced by the daily minimum and maximum temperatures respectively. $I_g$ is a direct and continuous measure of the current flowing between the anode and cathode due to the electrochemical reaction enabling a clear relationship between temperature and corrosion to be obtained. AE however detects corrosion through the energy emitted during the transient physical alterations that occur within the concrete microstructure, induced by the incompatibility between the corrosion oxides and the cement paste. Consequently, AE is not a direct measure of corrosion rate, but will be influenced by the rate and type of oxide production and its interaction with the concrete matrix.

The variance in AE energy reported in Section 3.1 could possibly be averaged out if the corrosion rate is kept constant for a fixed period of time, enabling correlation of AE Energy with $I_g$. This was the focus of the second part of the work, in which fixed temperatures, typical of various times of the year were replicated, and the corrosion rate was kept constant by providing a constant supply of water and maintaining a steady temperature.

### *3.2.1 Galvanic Current*

Varying the ambient temperature over a temperature range indicative of the UK seasonal climate induced changes in $I_g$ as shown in Figure 8, where the recorded $I_g$ for the second of the temperature cycles is plotted against actual room temperature which varied slightly from day to day.

From Figure 8 it is apparent that across the temperature range studied, $I_g$ increased by a factor of approximately 2.3 in each of the three corrosion cells. This might suggest that in the UK, the corrosion rate in real structures may also vary over this magnitude, assuming that the change in corrosion rate is only due to changes in temperature and that the internal moisture content of the concrete remains relatively constant.

### *3.2.2 Acoustic Hits*

Figure 9, presents the total number of AE hits per day at each recorded temperature for test one and two. The number of AE hits over time can be indicative of the level of activity occurring in a sample and it is apparent from Figure 9 that over the 24-hour periods where the control was emissive, it exhibited significantly lower AE activity in comparison to the corroding Cells. On most occasions, emission from the control over

a 24 hour period was practically zero. This confirms that the source of the emissions from the active cells arises mostly from the corrosion mechanism and not from sources in either the test method or testing environment. While there is no direct relationship evident between AE hits per day and temperature or $I_g$ (Figure 10), it is apparent that increasing the temperature tends to increase the range in number of AE hits per day. Furthermore the shortest and lowest range corresponds with the lowest temperature setting, which would suggest that acoustic activity is reduced at lower temperatures.

On completion of the tests Cells 1-3 were broken open and visually examined to investigate if there was any correlation between the number of hits and the extent of corrosion. A summary of the visual results, AE and $I_g$ is presented in Table 2, together with the total corrosion (Coulombs) calculated over the monitoring period. It is evident from Table 2 that all three cells had comparable areas of active corrosion (identified by the presence of oxides on the surface). Removal of the oxides revealed that in most instances a general type of corrosion had occurred with no obvious pits evident apart from a single pit of diameter 2.5 mm in Cell 1. There was evidence in all cases of oxide migration into the immediate cement paste. The number of active sites in Cell 2 was considerably lower than the other two Cells with the corrosion occurring on these sites having a larger build up of scale in comparison to the discrete corrosion sites that had occurred in the other two Cells. It is suggested that larger single areas of corrosion found in Cell 2 may have a higher concentration of currents, altering the local pH of the pore water and influencing the type of oxide being produced, thus the affecting the mobility of the oxide, volume of expansion and the AE.

No correlation was apparent between area of corrosion and AE hits or number of active sites. This would again suggest that the AE is a function of the interaction between the matrix and oxide.

*3.2.3 Acoustic Energy*

The total energy recorded over each 24-hour period was converted into energy per second and is presented in Figure 11 showing AE energy per second versus $I_g$ for Cells 1-3 for each of the temperature cycles. Even though in many circumstances $I_g$ was constant over a particular four-day period, the AE energy per hour (Figure 12) and between successive days was irregular. This supports the view that anodic dissolution is not the direct cause of emission, with the interaction of the expansive oxides with the matrix being a more plausible explanation. This mechanism has two implications. Firstly, at low corrosion rates the duration of monitoring will significantly influence the accuracy of detection; for example in Figure 12, which shows a 48 hour monitoring period from Cell 2 at 5$^{o}$C, monitoring between the 40-41$^{st}$ hour (high energy) and between the 20-21$^{st}$ hour (no energy) will give two very different results for the same corrosion rate and sample. Secondly, due to the irregular nature of the emission, only a couple of high-energy AE hits are required to distort the data collected within a 24 hour period, as shown by the two outliers in Figure 11.

For this reason, and as seen in Figure 11, there is no unique value of energy per second that corresponds to a given value of $I_g$, either within a Cell data set or between Cells. Furthermore, an increase in $I_g$ does not necessarily convert to an increase in AE energy per second. Thus, the total AE energy recorded over a finite period can only indicate an approximate range of corrosion activity. Due to the low corrosion rate,

only a relatively small number of processes occur within each 24 hour period, consequently the variations in energy that occur naturally between each micro fracture are not averaged out hence distorting the cumulative values.

Figure 13 shows AE Energy per second against temperature for Cells 1-4 where it is evident that the temperature and hence time of year, has apparently little influence on the ability of AE to detect corrosion of steel in concrete. Whilst the maximum energy per second increases at higher temperatures there is no clear relationship between temperature and AE Energy. This might also suggest that the change in $I_g$ induced by a change in temperature is not of a significant magnitude to induce any discernable change in the energy emitted.

*3.2.4 Half-cell Measurement (Seasonal Study)*

The half-cell evolution for Cells 1-4 is given in Table 3. Cells 1-2 exhibited an active potential over the entire test duration. Cell 4, (control) remained noble throughout both tests supporting the AE results presented, however some of the half-cell values fall within the intermediate range (-200 to -350mV), suggesting that a degree of water saturation was occurring. During the first test, Cell 3 indicated a potential that could either be noble or passive at both 5 and 15$^{o}$C. However, the AE results strongly suggest that corrosion was active as both the AE energy and AE hit rates were substantially higher than for the noble control. A similar result was reported by Li *et al* [23] who reported that AE could detect corrosion in concrete beams where the half-cell potential suggested that they were noble. The difference in half-cell potential values between test one and two is considered to be attributable to a time elapse of six months between tests.

No systematic changes between half-cell potential and temperature were observed, attributed to the lack of interdependence between the rate of corrosion and the half-cell potential. Factors such as a change in the water content and thus oxygen concentration are more likely to be contributory factors influencing the half-cell potential between test one and two.

## 4. Discussion

The acoustic emission technique has been shown to be an indirect measure of the corrosion rate, measuring the damage induced in the concrete by the production of expansive oxides. It has been demonstrated that AE is responsive to changes in daily temperature but not to 'seasonally' induced temperature changes which were held constant. It is therefore suggested that the increase in AE associated with the diurnal cycles is a response to the change in internal microclimate induced by the change in temperature and not due to an increase / decrease in the absolute steel corrosion rate. This notion is supported in Figure 14 showing the AE data obtained from Cell 3 whilst lowering the temperature in the static temperature room between tests. A clear increase in AE corresponding with the start of the reduction in temperature (which also reduced $I_g$) is evident. Once the temperature stabilised, the AE is returned to its original 'background' level. This pattern was also evident in the other two Cells. During this transition the control was silent suggesting that the increase in AE was not thermally induced. Consequently, if the increase in AE is as a result of an increase in $I_g$, the effect shown in Figure 14 would not have been apparent.

The mechanism behind this transitional increase in AE is not fully understood. However it is suggested that the increase in AE may be a result of changes in oxide composition, which may vary due to changes in water and oxygen content within the concrete matrix. As discussed in the Introduction, $RH_{int}$ is in constant non-equilibrium with the environment and in sheltered conditions, strongly influenced by temperature. Thus temperature-induced changes in $RH_{int}$ may result in a transitory increase in the availability of $O_2$ during a reduction in $RH_{int}$ or $H_2O$ during an increase in $RH_{int}$, enabling the formed oxides to undergo further reactions and increase in volume, thus exerting greater tensile forces within the concrete. Basheer and Nolan [7] have observed large variations in $RH_{int}$ corresponding to daily temperature variations, which would support this view. A second source of the emission may be the opening and closing of microcracks within the concrete, formed as a consequence of corrosion. However, further work is required to establish the exact mechanism.

Whilst the variations in energy/second within each cell have been discussed, variations in energy/second also exist between Cells shown in Figure 11. This may arise because the actual dissolution rate is unknown as micro-cell activity may be occurring on the anode. In this case $I_g$ is not equal to the dissolution current ($I_d$) of the metal, but equal to the cathodic current flowing from the chloride free sample [33]:

$$I_g = I_d - \left| I_c^A \right| = \left| I_c^C \right| \quad (1)$$

The dissolution current, therefore, must equal the total cathodic current:

$$I_d = I_a^A = \left| I_c^A \right| + \left| I_c^C \right| \quad (2)$$

From visual examination it was found that the corrosion in all Cells was localised, thus the corrosion rate in the samples is likely to be greater than the measured $I_g$. The significance of this error on the results is dependent upon the difference in the ratio of anodic/cathodic processes occurring on the anode, across the Cells, which from Table 2 is relatively equal (assuming areas without corrosion products are active cathodically).

The variation in corrosion rates resulting from seasonal temperature fluctuations was not clearly differentiated using AE within the scope of this work. Within real structures, the current density can range from 1 to 100 μm/cm$^2$ [34,35], depending upon the ratio of the anode to cathode area, resistivity of the concrete and oxygen availability. The increases in corrosion rates reported in this work are thus relatively small when put into context of the range of corrosion rates possible.

As an aside, the energy per second of similar beams corroding at 10 and 100 μm/cm$^2$ has been obtained from a selection of beams from previous work and another study [9,10], and are plotted in Figure 15 together with the data from Cells 1-3 which has been converted to current density by averaging the total galvanic current over the area of the anode and assuming that no micro-cell activity is occurring. Upholding the definitions of low, medium and high corrosion rates suggested by Andrade and Alonso [36], an empirical exponential relationship between corrosion rate and AE energy per second is apparent. Thus, the corrosion rates of the prisms monitored in the seasonal study can be classified as low to medium, offering a clear advantage over the half-cell, which only indicated a 90% probability of corrosion occurring in the beams.

It is acknowledged that AE cannot determine corrosion rate, as it is not an electrochemical technique but may indicate the rate of damage occurring to the concrete, which itself, is indirectly related to corrosion rate. It has also been demonstrated in this paper that AE is able to detect low rates of corrosion, in and in some instances where the half-cell potential is indicating borderline nobility. This is achievable through non-destructive testing and without perturbation of the corrosion reaction.

## 5. Significance

The findings of this work suggest that AE measurements taken on a structure exposed to an external environment are unlikely to be influenced by the time of year in which they were obtained, moreover corrosion induced AE is detectable over the range of temperatures likely to be encountered in the UK. However, the time of day of the test appears to impart a greater influence, possibly due to the short-term changes in microclimate that occur within the concrete.

It is clear from this work that when undertaking AE measurements on site a sufficient monitoring duration is required to average the high and low activity periods that exist due to the influence of temperature change in the diurnal cycles and stochastic nature of the emissions. Provided a suitable duration is determined, a reasonable and repeatable indication of corrosion damage may be obtainable. For example, the average energy per second values of Beams 1-3 over the five 24 hour periods were 0.069 (standard deviation (SD) = 0.018), 0.064 (SD = 0.018) and 0.164 (SD = 0.064)

respectively, which are comparable to the results of Cells 1-3, indicating a low corrosion rate (Figure15).

## 6. Conclusions

It has been shown that AE activity over a diurnal cycle mirrors the evolution of corrosion and temperature. It is suggested that this phenomenon is caused by changes in the internal microclimate of the concrete as it responds to variations in temperature. However, further work is suggested to investigate the exact cause of the emission. Consequently, if applying AE practically to determine the corrosion state of reinforcing steel exposed to an external environment any monitoring period must be of sufficient duration to enable the AE to be averaged out.

It was found that while different 'seasonal' temperatures influence the magnitude of $I_g$, the influence of the seasonal changes had an insignificant effect on the magnitude of AE. No AE was generated in the control sample by thermal cycling, suggesting that thermal cycling *per se* was not the cause of the AE.

No restrictions on the ability of AE to detect corrosion were found based on high or low temperatures. Furthermore AE has been shown to detect the damage occurring to the concrete induced by expansive oxides produced, even at low galvanic currents, when in some instances the half-cell potentials have indicated borderline nobility.

**Acknowledgements**

This work was undertaken at the Centre for Innovative Construction Engineering, Loughborough University. The authors acknowledge the financial assistance from the EPSRC and Balvac Whitley Moran Ltd in addition to specialist equipment loan and technical assistance from Physical Acoustics Limited. Atkins Consultants Ltd also gave assistance.

**References**


1. V. Zivica, L. Krajci, L. Bagel, M. Vargova, Const. Build. Mat. 11 (2) (1997) 99.
2. J.N. Envoldsen, C.M. Hansson, Cem. Conc. Res. 24 (7) (1994) 1373.
3. C. Andrade, C. Alonso, J. Sarria, Cem. Conc. Comp. 24 (2002) 55.
4. K. Tuutti, RILEM Quality Control of Concrete Structures, Stockholm, Sweden, (1979) 23.
5. T. Lui, R.W. Weyers, Cem. Conc. Res. 28 (3) (1998) 365.
6. L.J. Parrott, Mag. Conc. Res. 43 (151) (1991) 45.
7. P.A.M. Basheer, E. Nolan, Constr. Build. Mat. 15 (2001) 105.
8. A.M. Neville, Mater. Struct. 28 (1995) 63.
9. M.J. Ing, S.A. Austin, R. Lyons, Paper in submission to Cem. Conc. Res. October, 2002
10. S. A. Austin, R. Lyons, M.Ing, Paper accepted for pub. Corros. November, 2002.
11. A.G. Beattie, J. Acoustic Emission, 2 (1983) 95.
12. H. Mazille, R. Roathea, C. Tronel, Corros. Sci. 27 (9) (1995) 1365.
13. K. Matsuyama, A. Ishibashi, T. Fujiwara, S. Fukuchi, M. Ohtsu, Prog. Acoustic Emission, (1994) 361.
14. M. Shigeishi, S. Colombo, K.J. Broughton, H. Rutledge, A.J. Batchelor, M.C. Forde, Constr. Building Mater. 15 (2001) 35.
15. T.W. Rettig, M.J. Felsen, Corros. 32 (1976) 121.
16. F. Mansfield, P.J. Stocker, Corros. 35 (12) (1979) 541.
17. M. Fregonese, H. Idrissi, H. Mazille, L. Renaud, Y. Cetre, Corros. Sci. 43 (2001) 627.
18. M. Ohtsu, M. Shigeishi, H. Iwase, W. Koyanago, Mag. Concr. Res. 43 (155) (1991) 127.
19. A.S. Kobayashi, N.M. Hawkins, Y-L.A. Chan, I-J. Lin, Experi. Mech. (1980) 301.
20. Maji, S.P. Shah, Experi. Mech. (1988) 27.
21. K. Wu, B. Chen, W. Yao, Cem. Con. Res. 30 (2000) 1495.
22. S.W. Hearn, C.K.Shield, ACI Mat. J. 94 (6) (1997) 510.
23. Z. Li, S.P. Shah, ACI Mat. J. 91 (4) (1994) 372.
24. D-J. Yoon, W.J. Weiss, S.P. Shah, J. Engineering Mech. (2000) 273
25. S. Yuyama, T. Okamoto, M. Shigeishi, M. Ohtsu, T. Kishi, Acoustic Emission: Standards and Technology Update, ASTM STP 1353, S.J. Vahaviolos, Ed., American Society for Testing and Materials, West Conshohocken, PA, 1999.
26. S.E. Dunn, J.D. Young, W.H.Hartt, R.P. Brown, Corros. 40 (7) (1984) 339.
27. Z. Li, F. Li, A. Zdunek, E. Landis, S.P. Shah, ACI Mat. J. (1998) 68.
28. H. Idrissi, A.Limam, J. Acoustic Emission, 18 (2000) 307.
29. M.S. Weng, S.E. Dunn, W.H. Hartt, R.P. Brown, Corros. 38 (1) (1982) 9.
30. K.H.W. Seah, K.B. Lim, C.H. Chew, S.H. Teoh, Corros. Sci. 34 (10) (1993) 1707.
31. C. Andrade, J. Sarria, C. Alonso, Cem. Conc. Res. 29 (1999) 1249.
32. J.A. González, S. Felíu, P. Rodríguez, E.Ramírez, C. Alonso, C. Andrade, Mater. Struct. 29 (1996) 40.
33. F. Mansfeld, Corros. 27 (10) 1971.
34. C. Alonso, C. Andrade, J. Rodríguez, J.M. Diez, Mater. Struct. 31 (1998) 435.

35. J.A. González, C. Andrade, C. Alonso, S. Felíu, Cem. Conc. Res. 25 (2) (1995) 257.
36. C. Andrade, C. Alonso, Constr. Build. Mat. 15 (2001) 141.

## Figure Captions:



## List of Tables:

| Beam Number | Mass at start (kg) | Half-cell at start (mV/CSE) | Mass at end (kg) | Change in Mass (kg) | Half-Cell at End (mV/CSE) | Change in Half-Cell (mV/CSE) |
|---|---|---|---|---|---|---|
| 1 | 9.765 | -422 | 9.755 | -0.010 | -353 | 69 |
| 2 | 10.198 | -477 | 10.192 | -0.006 | -467 | 10 |
| 3 | 9.901 | -446 | 9.893 | -0.008 | -420 | 26 |
| 4 | 10.959 | -236 | 10.945 | -0.014 | -178 | 58 |

**Table 1** Half Cell Potential and Mass Changes, Beams 1-4

| Temperature (°C) | Test Number | Half-Cell Potential (mV/CSE) | | | |
|---|---|---|---|---|---|
| | | Cell 1 | Cell 2 | Cell 3 | Cell 4 |
| 25 | 1 | -490 | -381 | -421 | -200 |
| 15 | 1 | -465 | -385 | -349 | -269 |
| 5 | 1 | -447 | -368 | -350 | -114 |
| 5 | 2 | -521 | -478 | -481 | -205 |
| 10 | 2 | -424 | -494 | -492 | -235 |
| 25 | 2 | -538 | -512 | -489 | -202 |

**Table 3** Half Cell Potentials, Cells 1-4

| Cell | Average Hits / Day | Total Hits / Day | No. of corrosion sites | Area of corrosion products $cm^2$ | Average $I_g$ µA | Total Corrosion (Coulombs) | Maximum Pit Diameter (mm) |
|---|---|---|---|---|---|---|---|
| 1 | 50 | 1204 | 15 | 23.15 | 113.39 | 2290 | 2.5 |
| 2 | 76 | 1826 | 4 | 21.37 | 68.96 | 1380 | <1.0 |
| 3 | 50 | 1197 | 18 | 22.27 | 70.50 | 1421 | <1.0 |

**Table 2** Details of Corrosion Area and Number of Active Sites with and AE and Galvanic Current Results

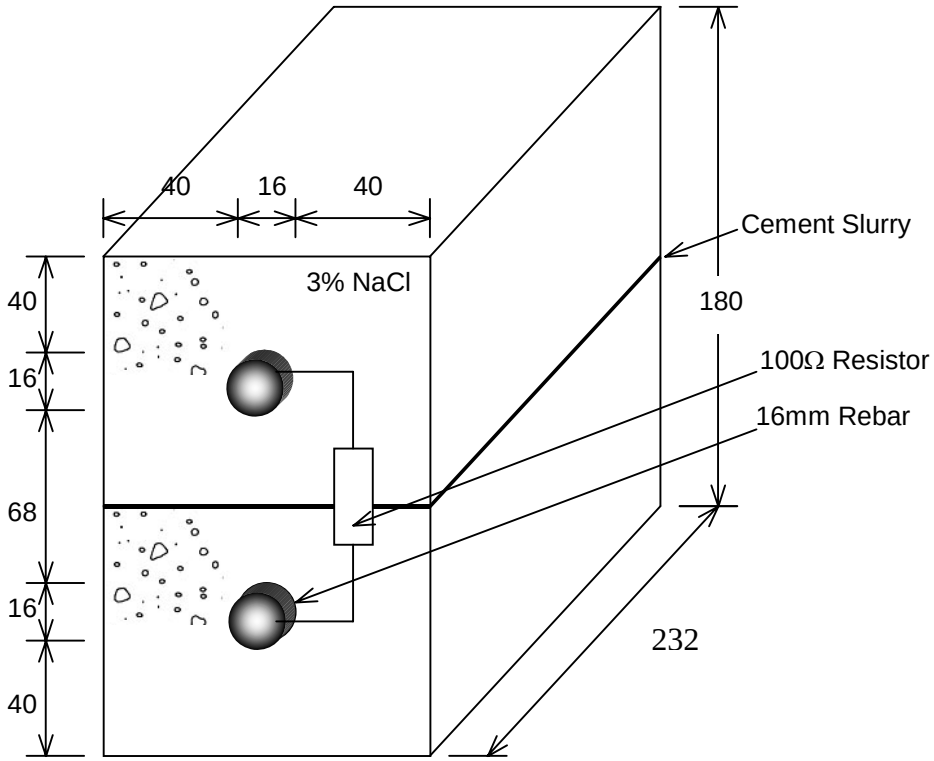


**Figure 1** Experimental Arrangement for the Diurnal Measurements

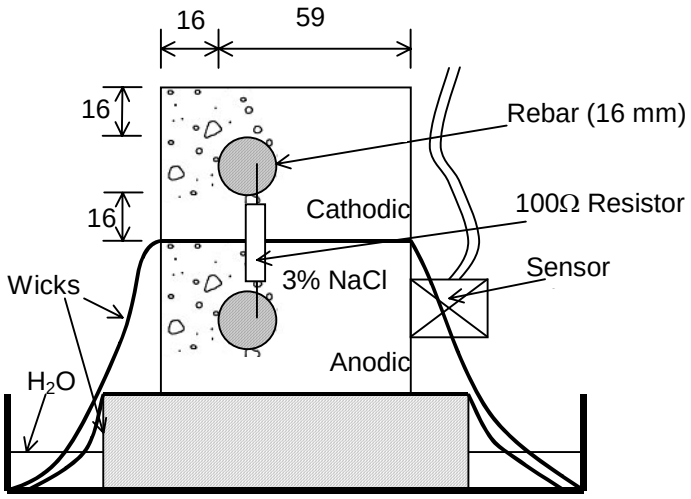


**Figure 2** Experimental Arrangement for Seasonal Cycling

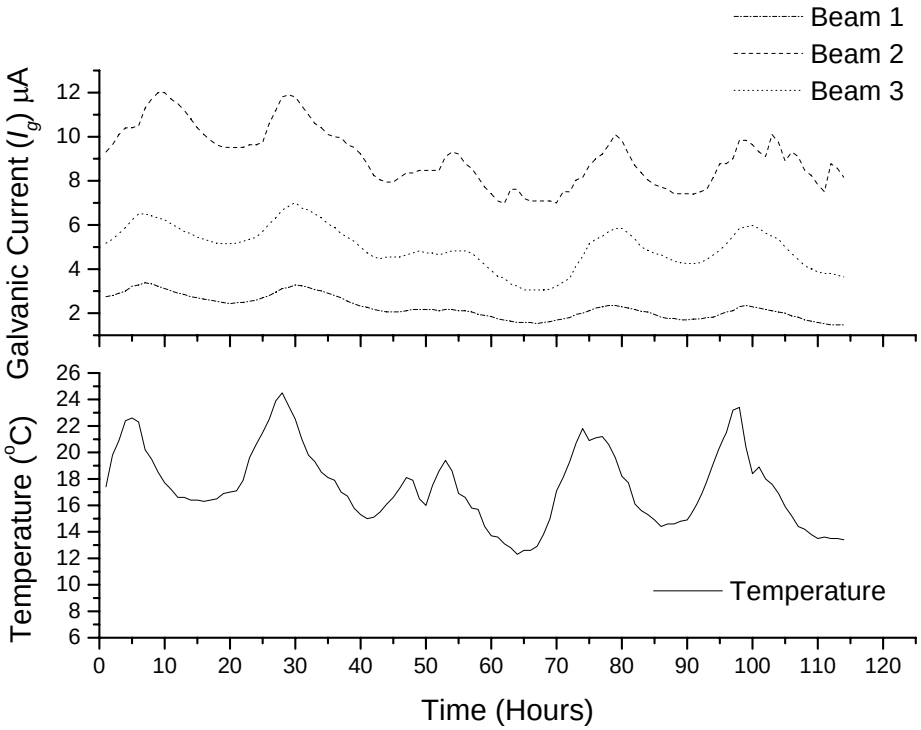


**Figure 3** Hourly Variations of (a) $I_g$ and (b) External Temperature

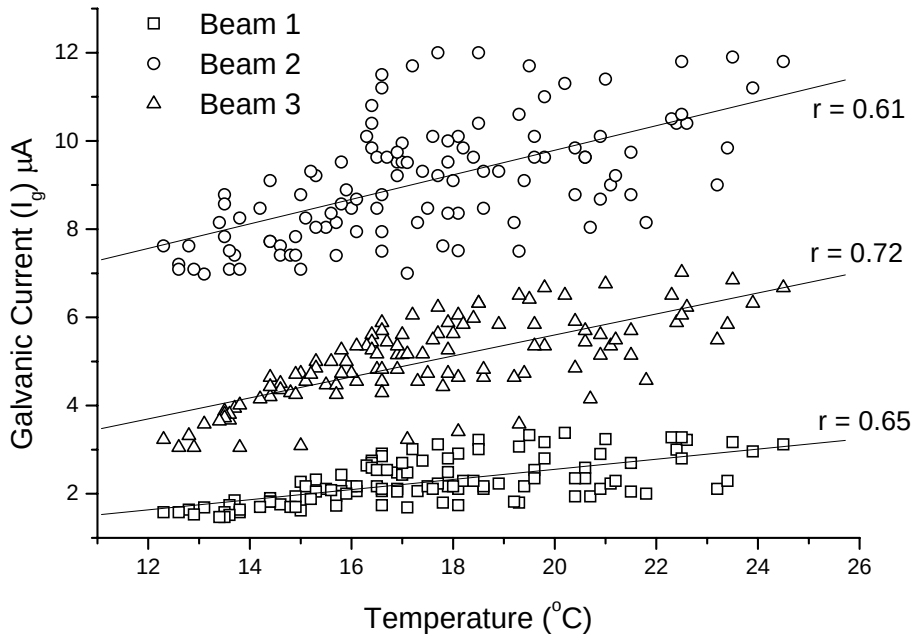


**Figure 4** Relationship between Galvanic Current and Temperature

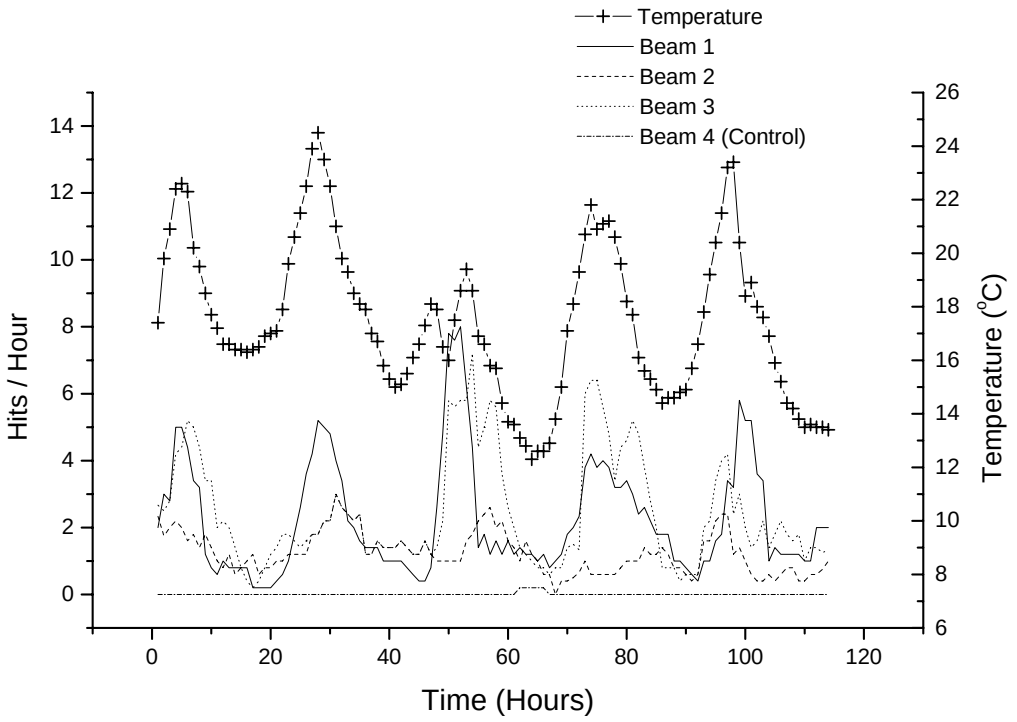


**Figure 5** AE Hits per Hour (Diurnal Cycle)

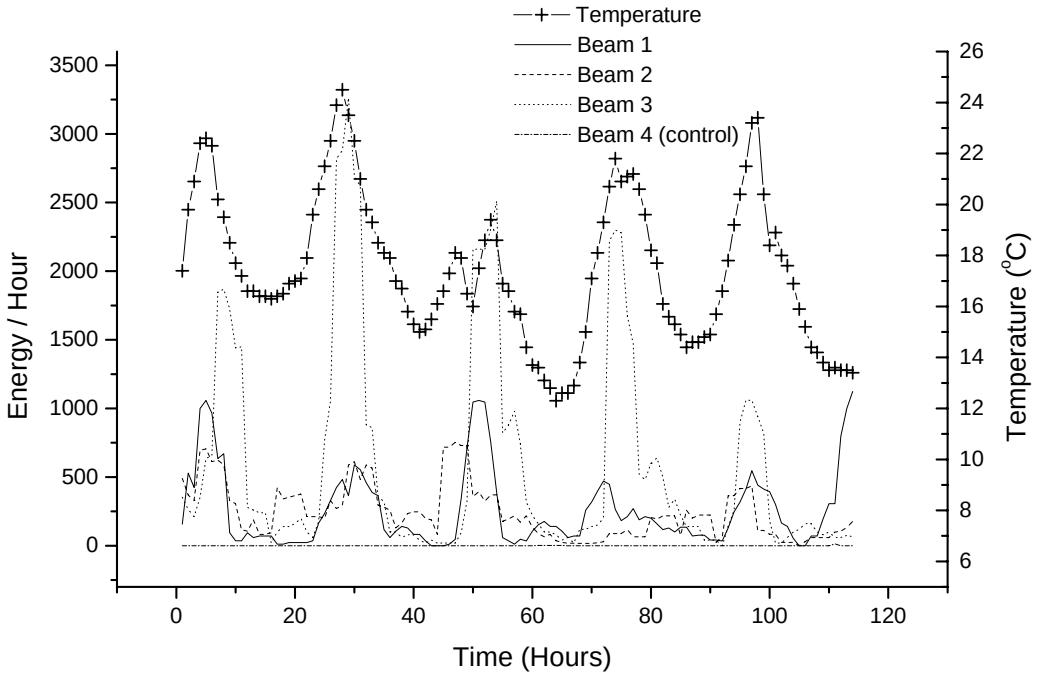


**Figure 6** AE Energy per Hour (Diurnal Cycle)

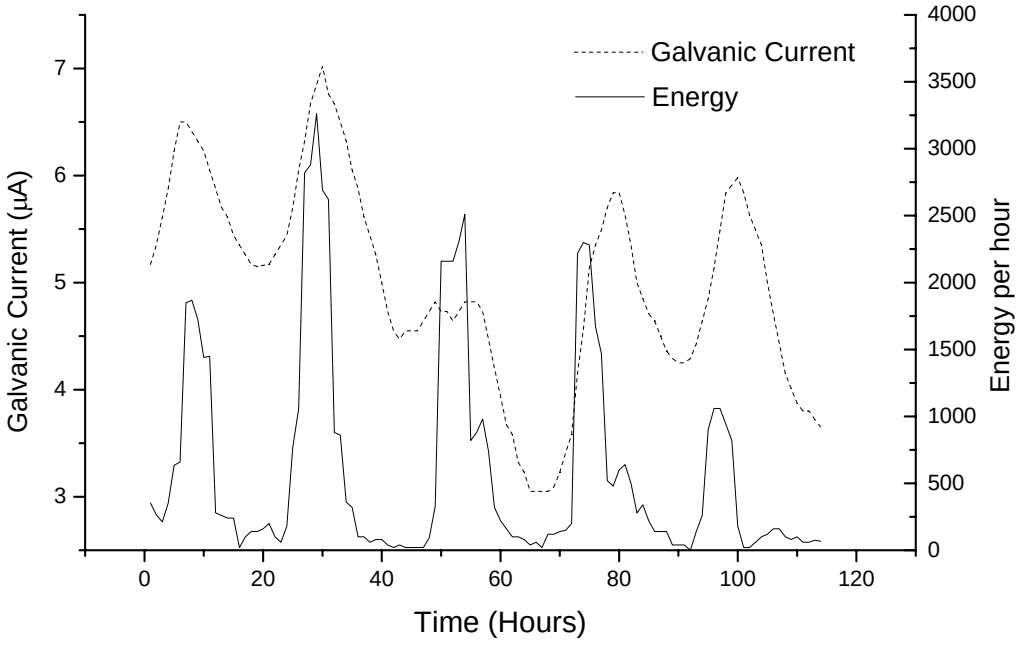


**Figure 7** Energy and Corrosion Rate for Beam 3.

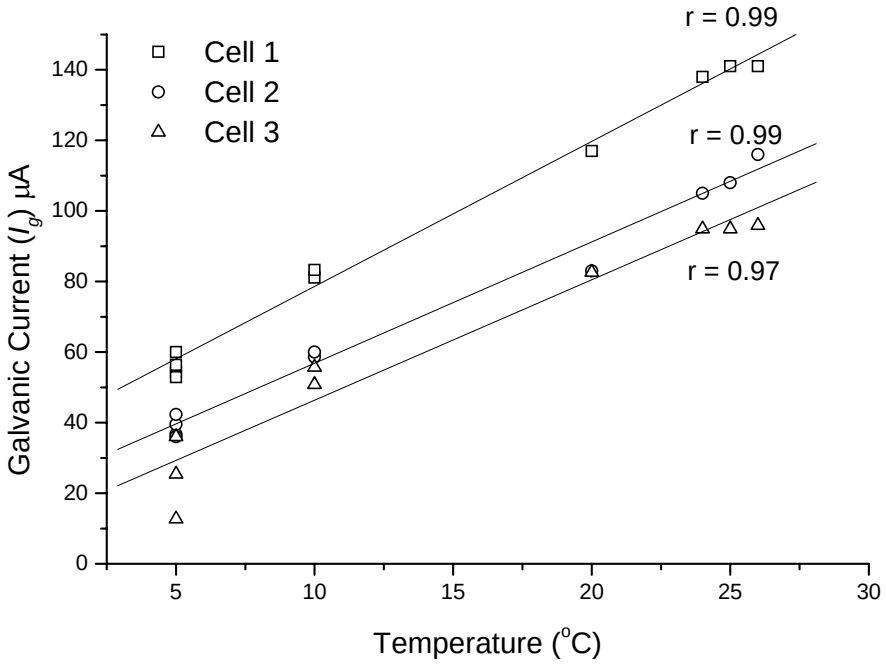


**Figure 8** Galvanic Current Versus Temperature (Seasonal Cycles)

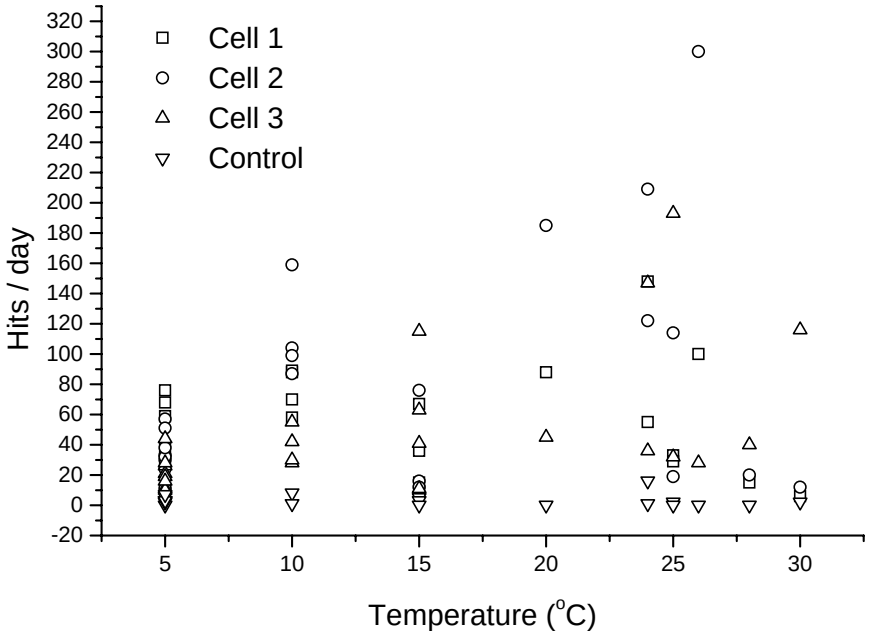


**Figure 9** Total AE Hits/Day for each Temperature

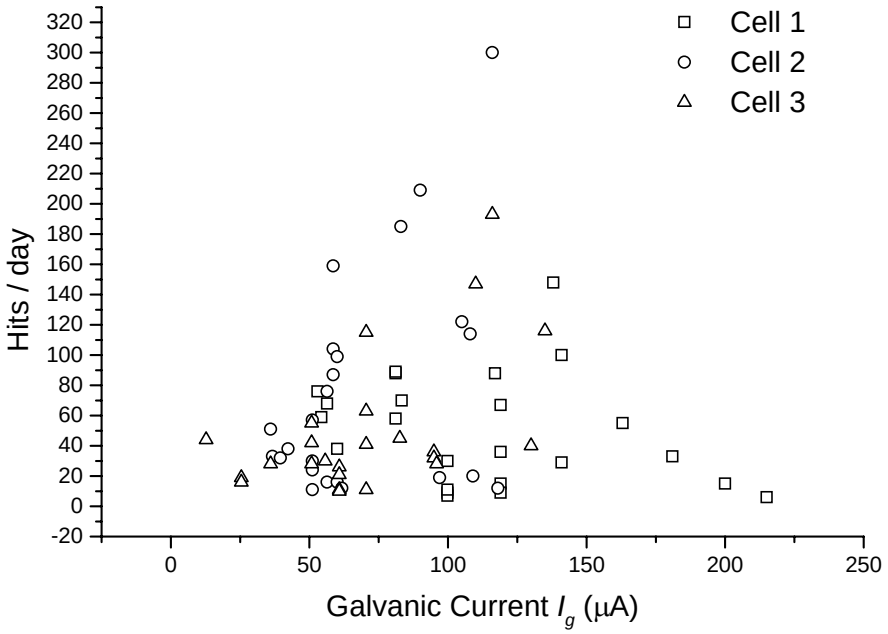


**Figure 10** Hits per Day Versus Galvanic Current.

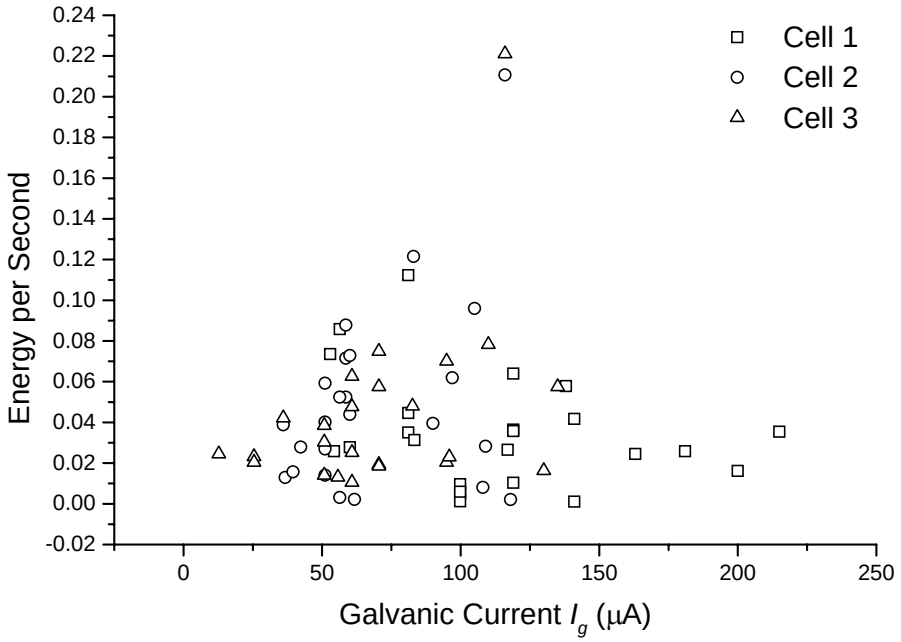


**Figure 11** Energy per Second Versus Galvanic Current

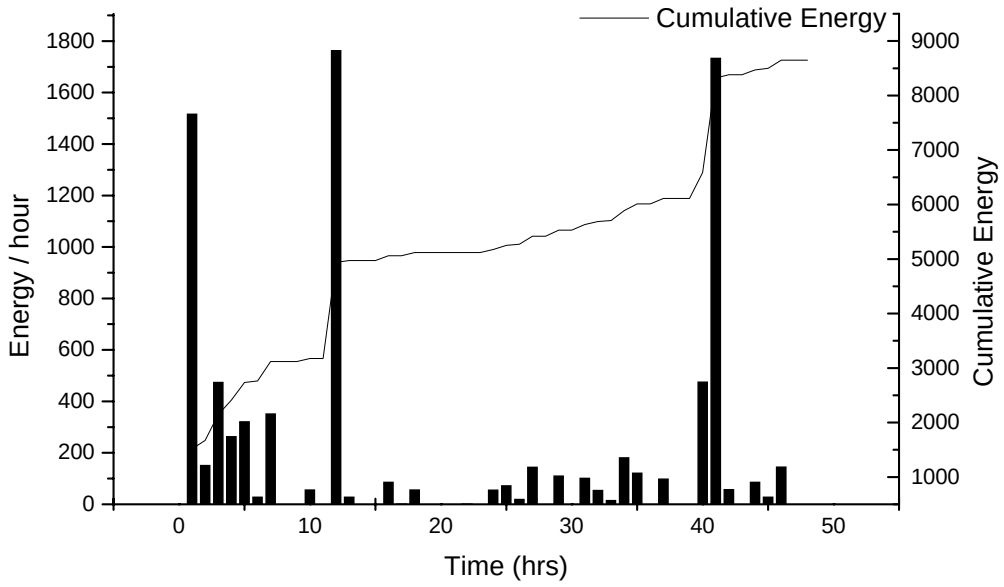


**Figure 12** Energy per Hour, Cell 3, 5°C.

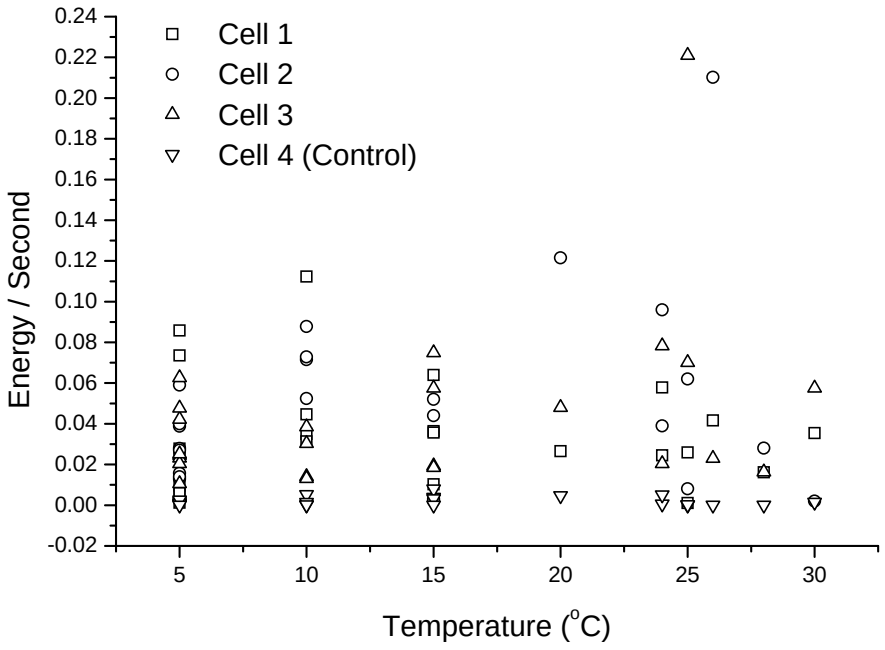


**Figure 13** Energy per Second Versus Temperature

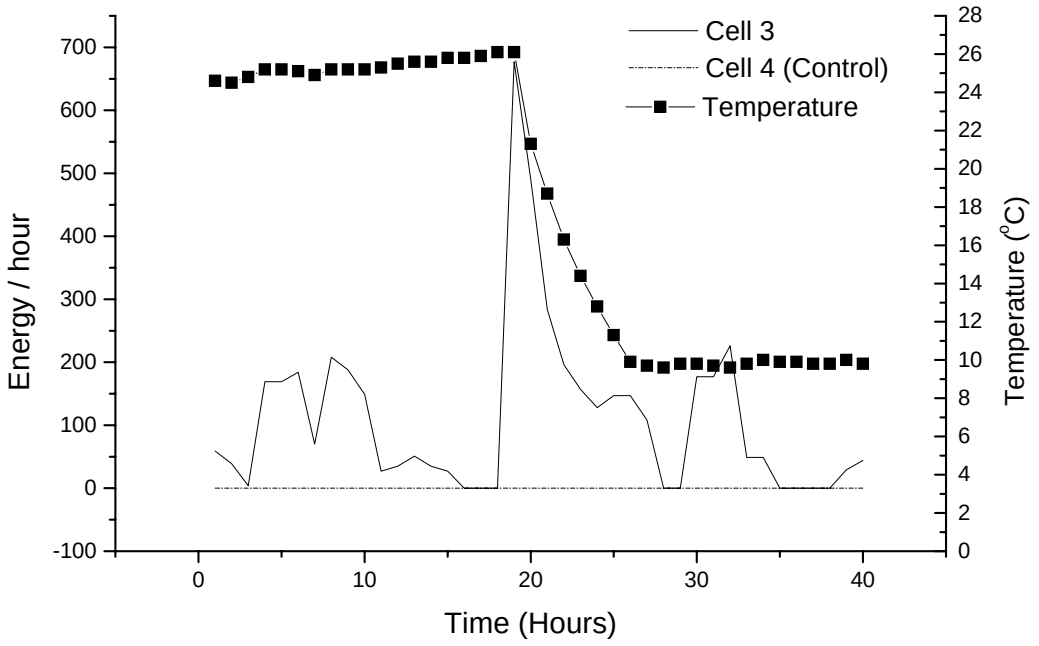


**Figure 14** Influence of Temperature Change on Energy Per Hour

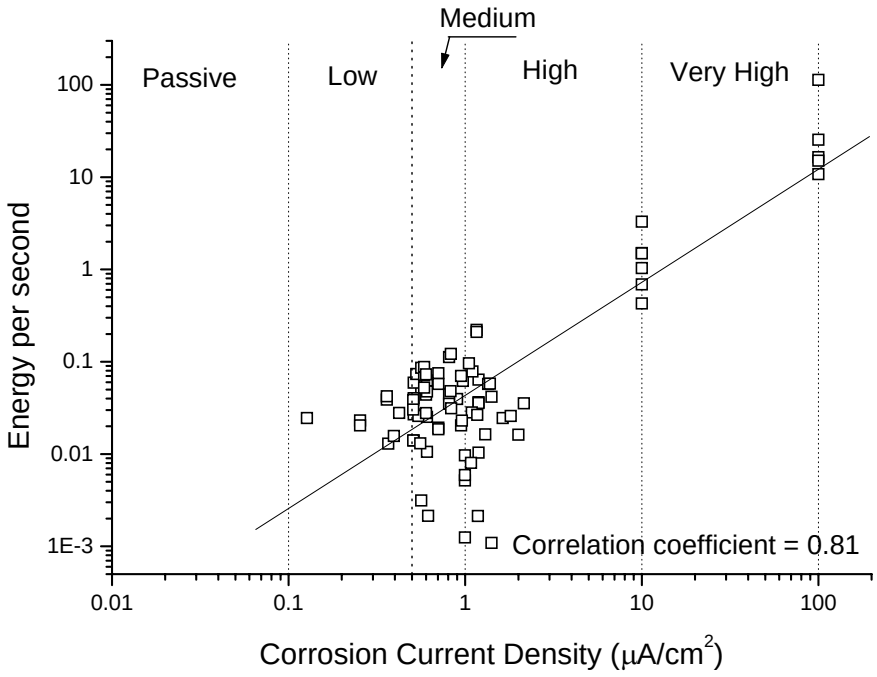


**Figure 15** Energy per Second for Different Corrosion Rates